

---

# Contrastive MIM: A Contrastive Mutual Information Framework for Unified Generative and Discriminative Representation Learning

---

Micha Livne  
NVIDIA  
mlivne@nvidia.com  
**WORKING DRAFT**

## Abstract

Learning representations that generalize well to unknown downstream tasks is a central challenge in representation learning. Existing approaches such as contrastive learning, self-supervised masking, and denoising auto-encoders address this challenge with varying trade-offs. In this paper, we introduce the *contrastive Mutual Information Machine* (cMIM), a probabilistic framework that augments the Mutual Information Machine (MIM) with a novel contrastive objective. While MIM maximizes mutual information between inputs and latent variables and encourages clustering of latent codes, its representations underperform on discriminative tasks compared to state-of-the-art alternatives. cMIM addresses this limitation by enforcing global discriminative structure while retaining MIM’s generative strengths.

We present two main contributions: (1) we propose cMIM, a contrastive extension of MIM that eliminates the need for positive data augmentation and is robust to batch size, unlike InfoNCE-based methods; (2) we introduce *informative embeddings*, a general technique for extracting enriched representations from encoder-decoder models that substantially improve discriminative performance without additional training, and which apply broadly beyond MIM.

Empirical results demonstrate that cMIM consistently outperforms MIM and InfoNCE in classification and regression tasks, while preserving comparable reconstruction quality. These findings suggest that cMIM provides a unified framework for learning representations that are simultaneously effective for discriminative and generative applications.

## 1 Introduction

Learning representations that remain effective across unknown downstream tasks is a central challenge in representation learning. Prominent approaches addressing this challenge include contrastive learning (*e.g.*, Chen et al. [2020], van den Oord et al. [2018]), self-supervised masking (*e.g.*, Devlin et al. [2018]), and denoising auto-encoders (*e.g.*, Bengio et al. [2013]).

In this work, we propose a new method, *cMIM* (Contrastive MIM), designed to learn representations that are broadly useful for downstream applications. cMIM integrates a contrastive learning objective with the Mutual Information Machine (MIM) framework introduced by Livne et al. [2019]. MIM is a probabilistic auto-encoder that maximizes mutual information between inputs and latent representations while clustering the latent codes. However, preliminary results suggest that MIM alone yields representations less effective for discriminative tasks compared to state-of-the-art alternatives. Our cMIM framework directly addresses this limitation by incorporating contrastive learning.

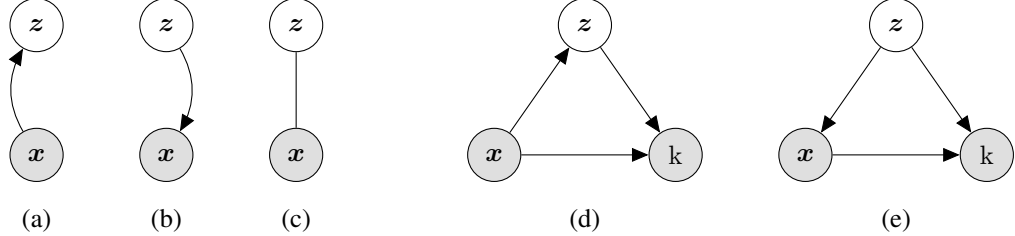


Figure 1: (Left) A MIM model learns two factorizations of a joint distribution: (a) encoding; (b) decoding factorizations; and (c) the estimated joint distribution (an undirected graphical model). (Right) We extend the MIM model with an additional binary variable  $k$ , and present the two factorizations of a joint distribution: (d) encoding; (e) decoding factorizations.

Our main contributions are as follows:

1. We propose a contrastive extension to the Mutual Information Machine (MIM) that enables learning discriminative representations without requiring data augmentation (no explicit “positive” pairs) and with reduced sensitivity to the number of negative samples (typically determined by batch size).
2. We introduce *informative embeddings*, a generic method for extracting embeddings from encoder–decoder models. This technique improves discriminative downstream performance without additional training and applies broadly to pre-trained encoder–decoder architectures.

By combining generative modeling with contrastive objectives, cMIM provides a unified framework effective for both generative and discriminative tasks. Empirical results show that cMIM produces representations that retain MIM’s generative capacity while significantly improving performance in downstream discriminative settings.

## 2 Formulation

In this section, we extend the formulation of the Mutual Information Machine (MIM), a probabilistic auto-encoder designed to learn informative and clustered latent codes. The clustering is achieved by minimizing the marginal entropy of the latent distribution over  $z$ , which results in latent codes that are closely positioned in Euclidean space for similar samples (see example in the work by Reidenbach et al. [2023]). In MIM, similarity between samples is defined by the decoding distribution, leading to a local structure around each latent code (*i.e.*, similar samples correspond to nearby latent codes). However, the global distribution of these latent codes, while aligned with a target or learned prior, may not be well-suited for discriminative tasks. To address this limitation, we propose augmenting the MIM objective with a contrastive objective term, which encourages the latent codes of dissimilar samples to be more distinct from each other. This modification aims to improve the global structure of the latent space, making it more suitable for discriminative downstream tasks. Throughout the paper,  $X$  denotes the observation and  $Z$  the latent codes.

### 2.1 Contrastive Learning

Contrastive learning is a representation learning technique that maximizes the similarity between positive pairs while minimizing the similarity between negative pairs. The similarity between samples is typically measured using a similarity function, such as cosine similarity  $s(z_i, z_j) = \frac{z_i \cdot z_j}{\|z_i\| \cdot \|z_j\|}$ . For example, in the InfoNCE loss van den Oord et al. [2018], the similarity is computed as the dot product of the normalized representations. More formally, we define the similarity of two samples  $x_i$  and  $x_j$  as  $s(z_i, z_j)$ , where the corresponding encoded representations are  $z_i = f_\theta(x_i)$ ,  $z_j = f_\theta(x_j)$ , and  $g(z_i, z_j) = \exp(s(z_i, z_j) / \tau)$  to be the exponent of the similarity scaled by scalar temperature  $\tau$ , and the InfoNCE loss per sample is defined as follows:

$$\text{InfoNCE}(x_i, x_i^+) = -\log \left( \frac{g(z_i, z_i^+)}{\sum_{j=1}^B g(z_i, z_j)} \right), \quad (1)$$

where  $\mathbf{x}_i^+$  is a positive augmentation of the same source sample, and  $\mathbf{x}_j$  are negative augmentation from different source samples. See van den Oord et al. [2018] for a detailed discussion on the InfoNCE loss.

In practice, the contrastive loss is formulated as a  $B$ -way classification problem, where the positive pair is distinguished as the first pair, and  $B$  represents the batch size. For effective learning, it is crucial that the data augmentation applied to the positive pair is meaningful; however, for certain modalities (*e.g.*, text), designing appropriate augmentations can be challenging. Furthermore, the effectiveness of the loss function is sensitive to the selection of negative examples and the batch size.

## 2.2 Contrastive MIM Learning (cMIM)

In this work, we propose augmenting the MIM objective with a contrastive term to introduce global discriminative structure to the locally clustered latent space. Specifically, we hypothesize that encouraging the latent codes of similar samples to be close to each other (*i.e.*, local structure) and the latent codes of dissimilar samples to be distinct (*i.e.*, global structure) are complementary objectives. When comparing MIM with its contrastive extension (cMIM), we expect cMIM to exhibit similar reconstruction fidelity, comparable clustering performance, and improved discriminative capabilities.

Contrastive learning typically relies on generating augmented data for positive pairs, introducing an inductive bias that may not capture all desired invariances within the data. Moreover, devising appropriate augmentations can be challenging for certain data modalities, such as text, as discussed in Le-Khac et al. [2020]. Additionally, contrastive learning is sensitive to batch size since it requires a sufficient number of negative examples to improve the quality of learned representations. Although contrastive methods that do not rely on negative examples exist—such as BYOL Grill et al. [2020]—these methods often introduce additional hyperparameters that can be difficult to tune.

### 2.2.1 Contrastive Learning without Data Augmentation

In this work, we propose to extend the MIM framework by introducing a new random variable  $k$  into MIM’s graphical model (Fig. 1b). Formally, the encoding (*i.e.*,  $q_{\theta}(\mathbf{x}, \mathbf{z}, k)$ ) and decoding (*i.e.*,  $p_{\theta}(\mathbf{x}, \mathbf{z}, k)$ ) factorizations of the joint distribution are defined as follows:

$$q_{\theta}(\mathbf{x}, \mathbf{z}, k) = q_{\theta}(k|\mathbf{x}, \mathbf{z}) q_{\theta}(\mathbf{z}|\mathbf{x}) q_{\theta}(\mathbf{x}) \quad (2)$$

$$p_{\theta}(\mathbf{x}, \mathbf{z}, k) = p_{\theta}(k|\mathbf{x}, \mathbf{z}) p_{\theta}(\mathbf{x}|\mathbf{z}) p_{\theta}(\mathbf{z}) \quad (3)$$

Let us first define  $\mathbf{z}_i$  as a latent code that is sampled from the joint encoding distribution  $q_{\theta}(\mathbf{x} = \mathbf{x}_i, \mathbf{z}, k = 1)$ , where given  $\mathbf{x}_i$ , we sample  $\mathbf{z}_i \sim q_{\theta}(\mathbf{z} | \mathbf{x}_i)$ . Here we introduced the random variable  $k$ , a binary variable representing the relationship between a sample  $\mathbf{x}_i$  and a latent code  $\mathbf{z}_j$ .  $k = 1$  for the paired sample  $(\mathbf{x}, \mathbf{z}) = (\mathbf{x}_i, \mathbf{z}_i)$  with  $\mathbf{z}_i \sim q_{\theta}(\mathbf{z} | \mathbf{x}_i)$ , and  $k = 0$  for mismatched pairs  $(\mathbf{x}_i, \mathbf{z}_j)$ ,  $j \neq i$ . As discussed below, introducing  $k$  allows the model to learn a contrastive objective without relying on data augmentation, which is typically required in contrastive learning. Choosing directional similarity (cosine) as the similarity function further encourages dissimilar samples to diverge in angle, while MIM’s original loss encourages similar samples to cluster in Euclidean space.

To elaborate, we define the discriminator distributions for the encoding and decoding factorizations over  $k$  as:

$$q_{\theta}(k | \mathbf{z} = \mathbf{z}_i, \mathbf{x}) = p_{\theta}(k | \mathbf{z} = \mathbf{z}_i, \mathbf{x}) = \text{Bernoulli}(k; p_{k=1}), \quad (4)$$

where

$$\begin{aligned} p_{k=1}(\mathbf{x}_i, \mathbf{z}_i) &= \frac{g(\mathbf{z}_i, \mathbf{z}_i)}{g(\mathbf{z}_i, \mathbf{z}_i) + \mathbb{E}_{\mathbf{x}' \sim \mathcal{P}(\mathbf{x}), \mathbf{z}' \sim q_{\theta}(\mathbf{z} | \mathbf{x}')} [g(\mathbf{z}_i, \mathbf{z}')] } \\ &\approx \frac{g(\mathbf{z}_i, \mathbf{z}_i)}{g(\mathbf{z}_i, \mathbf{z}_i) + \frac{1}{B-1} \sum_{\substack{j=1 \\ j \neq i}}^B g(\mathbf{z}_i, \mathbf{z}_j)} \end{aligned} \quad (5)$$

where  $g(\cdot, \cdot)$  is the exponentiated logits defined in Section 2.1, and  $s(\cdot, \cdot)$  is cosine similarity, and with  $\mathbf{x}' \neq \mathbf{x}_i$  when using in-batch approximation. We emphasize that both encoding and decoding distributions are identical, to further encourage consistency between the encoding and decoding distributions, in addition to the consistency promoted by MIM’s loss.

During training we always have  $k = 1$  since  $\mathbf{z}_i$  is sampled from the encoding distribution given  $\mathbf{x}_i$ . The expectation over other samples is approximated using the current batch of size  $B$ , excluding the current sample  $\mathbf{x}_i$ . This approach leads to simpler training procedure when compared to InfoNCE, and allows us to avoid the need for positive data augmentation, as we can directly compare the latent code  $\mathbf{z}_i$  with latent codes from other samples in the batch. See Algo. 1 for the training procedure of cMIM.

A key advantage of cMIM is reduced sensitivity to batch size. Moreover, since the sampling process guarantees  $k = 1$ , the model is never trained with  $k = 0$  samples, leading to a simplified empirical loss. By formulating the objective in terms of expectations—rather than a  $B$ -way classification as in standard contrastive loss—the expected similarity to other samples can be approximated efficiently via Monte Carlo sampling. This, in principle, decouples similarity estimation from batch size, making the method less sensitive to batch size as it grows, consistent with bounds from Hoeffding’s inequality [Hoeffding 1963].

Because our similarity  $s(\cdot, \cdot)$  is bounded (cosine similarity in  $[-1, 1]$  implies  $g(\cdot, \cdot) \in [e^{-1/\tau}, e^{1/\tau}]$ ), the in-batch Monte Carlo estimate concentrates around its expectation. In particular, Hoeffding’s inequality yields

$$\Pr\left(\left|\frac{1}{B-1} \sum_{j \neq i} g(\mathbf{z}_i, \mathbf{z}_j) - \mu\right| \geq \epsilon\right) \leq 2 \exp\left(-\frac{2(B-1)\epsilon^2}{(e^{1/\tau} - e^{-1/\tau})^2}\right). \quad (6)$$

Thus the estimator becomes more stable as  $B$  increases (variance  $\mathcal{O}(1/(B-1))$ ) Hoeffding [1963].

Another simplification is that cMIM requires no data augmentation, unlike conventional contrastive learning where augmentations are essential for defining positive pairs. In cMIM, clustering is already promoted by the MIM objective, removing this requirement. This avoids the often challenging design and tuning of augmentations, further reducing training complexity. The combination of clustered latent codes with discriminative angular structure yields a latent space with stronger discriminative structure.

### 2.2.2 Contrastive MIM and InfoNCE

To better understand the proposed contrastive loss, we can relate it to the InfoNCE loss. In InfoNCE, the positive pair is defined by data augmentation, encourages the model to maximize the similarity between augmented samples and minimize the similarity for other samples. In contrast, MIM already clusters similar samples in latent space, and the contrastive term is used to encourage dissimilar samples to be more distinct from each other. We can rewrite Eq. (5) as follows:

**Relation to InfoNCE** Let  $s_{ij} \triangleq s(\mathbf{z}_i, \mathbf{z}_j) / \tau$  so that  $g(\mathbf{z}_i, \mathbf{z}_j) = \exp(s_{ij})$ . From Eq. (5) we have

$$\begin{aligned} p_{k=1} &= \frac{\exp(s_{ii})}{\exp(s_{ii}) + \frac{1}{B-1} \sum_{j \neq i} \exp(s_{ij})} \\ &= \frac{(B-1) \exp(s_{ii})}{(B-1) \exp(s_{ii}) + \sum_{j \neq i} \exp(s_{ij})} \\ &= \frac{\exp(s_{ii} + \log(B-1))}{\exp(s_{ii} + \log(B-1)) + \sum_{j \neq i} \exp(s_{ij})}. \end{aligned} \quad (7)$$

**Proposition.** The probability  $p_{k=1}$  above equals the softmax over the  $B$  candidates  $\{\mathbf{z}_i, \{\mathbf{z}_{j \neq i}\}\}$  where the *positive* logit is shifted by a constant  $\log(B-1)$ :

$$p_{k=1} = \text{softmax}\left(\left[s_{ii} + \log(B-1), \{s_{ij}\}_{j \neq i}\right]\right)_{\text{pos}}.$$

Consequently, minimizing  $-\log p_{k=1}$  is identical to an InfoNCE cross-entropy computed on logits  $\{s_{ii} + \log(B-1), s_{ij} (j \neq i)\}$ , i.e., InfoNCE with a fixed positive-logit offset.

---

**Algorithm 1** Learning parameters  $\theta$  of cMIM

---

**Require:** Samples from dataset  $\mathcal{P}(\mathbf{x})$

- 1: **while** not converged **do**
- 2:  $\mathcal{D} \leftarrow \{\mathbf{x}_j, \mathbf{z}_j \sim q_{\theta}(\mathbf{z}|\mathbf{x})\mathcal{P}(\mathbf{x})\}_{j=1}^B$  {Sample a batch of size  $B$ }
- 3:  $\hat{\mathcal{L}}_{\text{A-MIM}}(\theta; \mathcal{D}) = -\frac{1}{B} \sum_{i=1}^B \left( \log p_{\theta}(\mathbf{x}_i|\mathbf{z}_i) + \log p_{k=1}(\mathbf{x}_i, \mathbf{z}_i) \right. \\ \left. + \frac{1}{2} (\log q_{\theta}(\mathbf{z}_i|\mathbf{x}_i) + \log \mathcal{P}(\mathbf{z}_i)) \right)$
- 5:  $\Delta\theta \propto -\nabla_{\theta} \hat{\mathcal{L}}_{\text{A-MIM}}(\theta; \mathcal{D})$  {Gradient computed through sampling using reparameterization}
- 6: **end while**

---

Figure 2: Training algorithm for cMIM.

**Remarks.** (i) *Calibration.* If all logits are equal ( $s_{ij} = s_{ii}$ ), then  $p_{k=1} = 1/2$  (independent of  $B$ ), whereas standard InfoNCE (unshifted softmax with  $\sum_{j=1}^B \exp(s_{ij})$  in the denominator) yields  $p_{k=1} = 1/B$ . (ii) *Gradient shape.* With cosine similarity,  $s_{ii} = 1/\tau$  is constant, so the positive contributes no gradient and the gradients originate solely from the negative mean; local attraction (*i.e.*, clustering) is provided by the MIM term. (iii) *Exact InfoNCE and MI bound.* If the mean over negatives in Eq. (5) is replaced by the *sum* (*i.e.*, drop the factor  $1/(B-1)$ ), the offset disappears and one recovers standard InfoNCE  $\frac{\exp(s_{ii})}{\sum_{j=1}^B \exp(s_{ij})}$  together with the classical  $I(X; Z) \geq \log B - \mathbb{E}[\mathcal{L}_{\text{InfoNCE}}]$  bound. We point the reader to van den Oord et al. [2018] for a detailed discussion on the optimum of the InfoNCE loss.

**Differences from InfoNCE** Since cMIM does not rely on data augmentation, it does not require the positive pair to be defined by augmentations. Instead, the positive pair is defined by the latent code  $\mathbf{z}_i$  sampled from the encoding distribution given  $\mathbf{x}_i$ . This allows cMIM to avoid the challenges associated with designing appropriate augmentations for different modalities, such as text, where augmentations can be difficult to define.

In addition, our mean-denominator form calibrates the positive probability at  $p_{k=1} = 1/2$  when logits are equal (independent of  $B$ ), and the rapid convergence of the expectation estimator makes cMIM more robust to variations in batch size, as it does not strongly rely on the number of negative samples. We support this claim with empirical results in Section 3. We also note that the different calibration prevents cMIM from enjoying the classical InfoNCE mutual information bound. However, cMIM does inherit MIM’s mutual information bound (see Livne et al. [2019]), which is sufficient for learning informative latent codes.

That said, the quality of the Monte Carlo estimator and the diversity of negatives still improve with larger batches (or a memory queue). Empirically, we observe reduced calibration sensitivity but still a monotonic gain from increasing the effective number of negatives.

### 2.2.3 cMIM Training Procedure

The training of cMIM is conducted using the MIM objective applied to the extended graphical model, as discussed in Livne et al. [2019]. Specifically, MIM is defined over a mixture model as follows:

$$\mathcal{M}_{\theta}(\mathbf{x}, \mathbf{z}, \mathbf{k}) = \frac{1}{2} (p_{\theta}(\mathbf{k} | \mathbf{z}, \mathbf{x}) p_{\theta}(\mathbf{x} | \mathbf{z}) p_{\theta}(\mathbf{z}) + q_{\theta}(\mathbf{k} | \mathbf{z}, \mathbf{x}) q_{\theta}(\mathbf{z} | \mathbf{x}) q_{\theta}(\mathbf{x})), \quad (8)$$

with a sampling distribution  $\mathcal{M}_{\mathcal{S}}(\mathbf{x}, \mathbf{z}, \mathbf{k})$ , given by

$$\mathcal{M}_{\mathcal{S}}(\mathbf{x}, \mathbf{z}, \mathbf{k}) = \frac{1}{2} (p_{\theta}(\mathbf{k} | \mathbf{z}, \mathbf{x}) p_{\theta}(\mathbf{x} | \mathbf{z}) \mathcal{P}(\mathbf{z}) + q_{\theta}(\mathbf{k} | \mathbf{z}, \mathbf{x}) q_{\theta}(\mathbf{z} | \mathbf{x}) \mathcal{P}(\mathbf{x})), \quad (9)$$

as discussed in Livne et al. [2019], where we introduce here the discriminator distributions over  $\mathbf{k}$ .

The learning process for MIM involves minimizing an upper bound, defined as follows:

$$\begin{aligned} \mathcal{L}_{\text{MIM}}(\theta) &= \frac{1}{2} \left( CE(\mathcal{M}_{\mathcal{S}}(\mathbf{x}, \mathbf{z}, \mathbf{k}), q_{\theta}(\mathbf{x}, \mathbf{z}, \mathbf{k})) \right. \\ &\quad \left. + CE(\mathcal{M}_{\mathcal{S}}(\mathbf{x}, \mathbf{z}, \mathbf{k}), p_{\theta}(\mathbf{x}, \mathbf{z}, \mathbf{k})) \right) \\ &\geq H_{\mathcal{M}_{\mathcal{S}}}(\mathbf{x}, \mathbf{k}) + H_{\mathcal{M}_{\mathcal{S}}}(\mathbf{z}) - I_{\mathcal{M}_{\mathcal{S}}}(\mathbf{x}, \mathbf{k}; \mathbf{z}) \end{aligned} \quad (10)$$

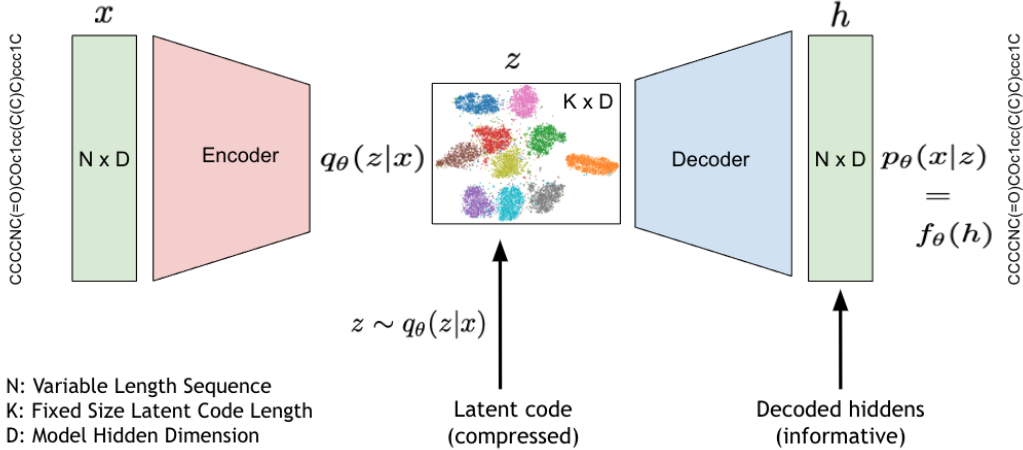


Figure 3: Informative embeddings  $h$  are extracted from an input observation  $x$  by taking the output from the decoder’s hidden states, prior to their mapping to the parameters of the decoding distribution  $p_\theta$ . Teacher forcing should be applied when necessary, particularly in the case of auto-regressive distributions.

where we treat  $k, x$  as a single observed variable during training, and remind the reader that  $k = 1$  for all samples  $x$  Livne et al. [2019].

We also provide an explicit example of the loss for A-MIM, an asymmetric version of MIM, as discussed in Livne et al. [2019]. In A-MIM we sample  $(x, z, k)$  from the encoding path but evaluate cross-entropies under both factorizations:

$$\mathcal{L}_{\text{A-MIM}}(\theta) = -\frac{1}{2} \mathbb{E}_{x \sim \mathcal{P}(x), z \sim q_\theta(z|x), k=1} \left[ \begin{aligned} & \log p_\theta(k|z, x) + \log p_\theta(x|z) + \log p_\theta(z) \\ & + \\ & \log q_\theta(k|z, x) + \log q_\theta(z|x) + \log q_\theta(x) \end{aligned} \right] \quad (11)$$

where we extend the loss from Livne et al. [2019] by incorporating  $k$  into the joint distribution.

The training algorithm for cMIM is presented in Algorithm 1, where we extend the learning procedure from Livne et al. [2020]. The final empirical loss is defined below:

$$\begin{aligned} \hat{\mathcal{L}}_{\text{A-MIM}}(\theta; \mathcal{D}) = & -\frac{1}{N} \sum_{i=1}^N \left( \log p_\theta(x_i|z_i) + \log p_{k=1}(x_i, z_i) \right. \\ & \left. + \frac{1}{2} (\log q_\theta(z_i|x_i) + \log \mathcal{P}(z_i)) \right) \end{aligned} \quad (12)$$

where  $\mathcal{D} = \{x_i, z_i \sim q_\theta(z|x)\}_{i=1}^N$  is the sample set,  $p_{k=1}$  is defined in Eq. (5),  $p_{k=1}$  is used for both the encoding and decoding distributions, and the anchor  $\mathcal{P}(z_i) = \mathcal{N}(z = z_i | \mu = 0, \sigma = 1)$  is a diagonal Normal distribution.

### 2.3 Informative Embeddings

Inspired by the success of leveraging output hidden states from various layers (e.g., Zeng et al. [2024]) of GPT-based large language models (LLMs, see Brown et al. [2020]) for downstream tasks, and recognizing the limitations of using such hidden states without further fine-tuning (e.g., NV-Embed by Lee et al. [2024]), we propose a generic method to enhance the quality of embeddings extracted from the MIM model, as depicted in Fig. 3.

Specifically, the embeddings  $h$  are extracted from the hidden states of the decoder, just before they are mapped to the parameters of the decoding distribution  $p_\theta(x | z) = f_\theta(h)$ . These embeddings are then utilized for various downstream tasks, including classification, clustering, and generation.

For auto-regressive distributions, such as text, teacher forcing is employed, where the input  $x$  is fed into both the encoder and decoder, eliminating the need to generate the next token. For non-auto-regressive distributions, such as images, there is no need for teacher forcing, and the embeddings

$\mathbf{h}$  are directly used for tasks like classification or clustering. More formally, the embeddings  $\mathbf{h}_i$  for sample  $\mathbf{x}_i$  are defined as:

$$\mathbf{h}_i = \text{Decoder}(\mathbf{x}_i | \mathbf{z}_i \sim q_{\theta}(\mathbf{z} | \mathbf{x}_i)) = \text{Decoder}(\mathbf{x}_i, \text{Encoder}(\mathbf{x}_i)), \quad (13)$$

where the above equation is employing teacher forcing for auto-regressive distributions.

We propose that instead of directly using the latent codes from MIM for downstream tasks, the focus should be on the embeddings  $\mathbf{h}$  derived from the decoder's hidden states. As we demonstrate, these embeddings are crucial for downstream tasks and are adapted according to the specific characteristics of the data, whether auto-regressive or non-auto-regressive. We note that informative embeddings can be extracted from any encoder-decoder model, not just MIM.

To illustrate the intuition behind using informative embeddings, consider the case of text generation. The embeddings  $\mathbf{h}_i$ , extracted from the decoder's hidden states by averaging over the sequence dimension, encapsulate information from the latent code that has been transformed to represent the probability distribution of the next token. This can be viewed as an "enriched" representation of the latent code, augmented with additional contextual information from the decoder, resulting in a more comprehensive representation of the observation (*i.e.*, capturing the entire distribution rather than just the actual observation). By leveraging these enriched embeddings for downstream tasks, we can exploit the additional information contained in the decoder's hidden states, potentially enhancing performance in discriminative tasks such as classification or regression. Unless stated otherwise, for sequences we mean-pool decoder hidden states to obtain  $\mathbf{h}_i \in \mathbb{R}^d$ ; gradients flow through both encoder and decoder during cMIM training.

### 3 Experiments

To evaluate the proposed cMIM model, we conduct experiments on a 2D toy example, MNIST-like images, and on molecular property prediction tasks (MolMIM by Reidenbach et al. [2023]). The 2D toy example illustrates the impact of the proposed contrastive MIM loss. We then explore the qualitative nature of cMIM by running rigorous experiments on MNIST-like datasets. Finally, we compare the performance of cMIM with MIM, VAE, and AutoEncoder models trained on molecular data, assessing their reconstruction and effectiveness in downstream tasks.

#### 3.1 Experiment Details and Datasets

#	Dataset	Train Samples	Test Samples	Categories	Description
1	MNIST	60,000	10,000	10	Handwritten digits
2	Fashion MNIST	60,000	10,000	10	Clothing images
3	EMNIST Letters	88,800	14,800	27	Handwritten letters
4	EMNIST Digits	240,000	40,000	10	Handwritten digits
5	PathMNIST	89,996	7,180	9	Colon tissue histology
6	DermaMNIST	7,007	2,003	7	Skin lesion images
7	OCTMNIST	97,477	8,646	4	Retinal OCT images
8	PneumoniaMNIST	9,728	2,433	2	Pneumonia chest X-rays
9	RetinaMNIST	1,600	400	5	Retinal fundus images
10	BreastMNIST	7,000	2,000	2	Breast tumor ultrasound
11	BloodMNIST	11,959	3,432	8	Blood cell microscopy
12	TissueMNIST	165,466	47,711	8	Kidney tissue cells
13	OrganAMNIST	34,581	8,336	11	Abdominal organ CT scans
14	OrganCMNIST	13,000	3,239	11	Organ CT, central slices
15	OrganSMNIST	23,000	5,749	11	Organ CT, sagittal slices

Table 1: **Image Classification:** Summary of train/test samples, categories, and descriptions for MNIST, EMNIST, and MedMNIST datasets.

All models are trained in an unsupervised manner. The checkpoint with the lowest validation loss is selected for evaluation. We avoid selecting any intermediate checkpoints, a common heuristic which does not scale well with complexity and model size. For downstream tasks, we freeze the

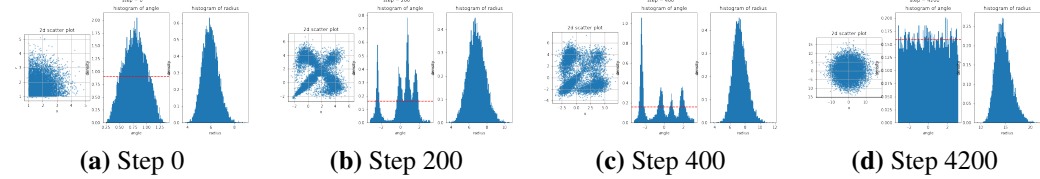


Figure 4: Effect of the contrastive MIM loss term in Eq. (5) on the 2D toy example. Each plot shows: latent space (left), histogram of latent code angles (middle), and histogram of latent radii (right). From (a) initialization in the first quadrant to (d) after 4200 training steps, the loss distributes points uniformly in angle while allowing radii to vary. This complements MIM’s clustering by encouraging angular uniformity, which enhances separability and thus improves downstream discriminative performance.

encoder-decoder and train lightweight classifiers on the learned representations, evaluating them on the held-out test set. Importantly, classification accuracy is not monitored during training. This ensures that comparisons reflect the quality of unsupervised representations rather than reliance on checkpoint selection heuristics. Training continues until convergence, making comparisons fair across models.

**2D Toy Example.** A synthetic dataset of 1000 points in 2D space is initialized in the first quadrant. The task is to check the effect of the proposed contrastive MIM loss on their position, highlighting the effect of Eq. (5).

**Image Classification on MNIST-like Datasets.** We train MIM, cMIM, VAE, cVAE (VAE with the contrastive term), and InfoNCE to convergence on MNIST-like datasets. Comparisons include classification accuracy, batch size sensitivity, and reconstruction (except InfoNCE). Datasets include MNIST Deng [2012], EMNIST (letters, digits) Cohen et al. [2017], and MedMNIST Yang et al. [2021]. All images are resized to  $28 \times 28$  pixels and converted to black and white when needed. We used  $\tau = 0.1$  (as in InfoNCE) following a small hyper-parameter search with  $\tau \in \{0.1, 1\}$ . The encoder is a Perceiver Jaegle et al. [2021] with 1 cross-attention layer, 4 self-attention layers, hidden size 16, projecting 784 pixels to 400 steps, followed by a projection to 64-dimensional latent codes. The decoder mirrors this design. Models are trained for 500k steps with batch sizes 2, 5, 10, 100, 200, using Adam with learning rate  $10^{-3}$ , and WSD scheduler Hu et al. [2024]. Classifiers include KNN ( $k = 5$ ; cosine and Euclidean metrics) and a one-hidden-layer MLP (size 400, Adam,  $10^{-3}$ , 1000 steps).

**Molecular Property Prediction.** We use ZINC-15 Sterling and Irwin [2015] with SMILES Weininger [1988] sequences, following Reidenbach et al. [2023]. Properties include ESOL, FreeSolv, and Lipophilicity. Here  $\tau = 1$ . Both MIM and cMIM are trained for 250k steps. Embeddings are evaluated using SVM and MLP regressors, both with and without informative embeddings, and compared against CDDD Winter et al. [2019]. Architectural details appear in Appendix A.

### 3.2 Effects of cMIM Loss on 2D Toy Example

We study the effect of the proposed contrastive MIM loss term (Eq. (5)) on a 2D toy example. Training minimizes the negative log-likelihood associated with Eq. (5), learning optimal latent codes in two dimensions. Here we use  $\tau = 1$ .

We expect the latent codes to distribute uniformly across all angles while maintaining variability in radii, as suggested by Wang and Isola [2020]. Fig. 4 shows the progression of the latent space during training. The results confirm that the contrastive term integrates smoothly with the MIM objective, preserving radial clustering while enforcing uniform angular distribution.

### 3.3 Classification Accuracy

We now analyze classification accuracy, as a proxy for the quality of the learned embeddings, and which was never used as a training signal.

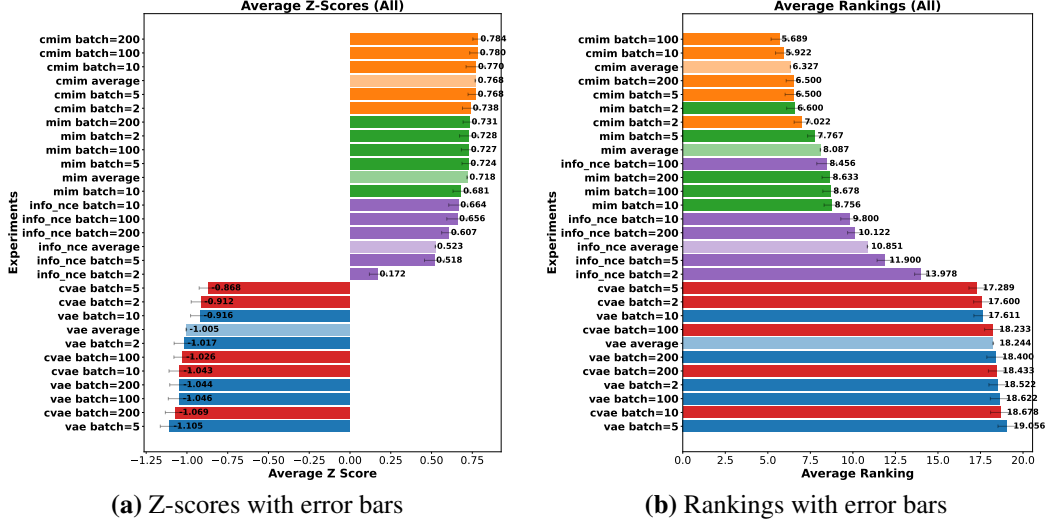


Figure 5: Classification accuracy across datasets and classifiers. Colors indicate model families: cMIM (orange), MIM (green), InfoNCE (purple), VAE (blue), cVAE (red). Light shades denote model averages. cMIM consistently outperforms all baselines across batch sizes and metrics.

Model (Latent K × D)	ESOL		FreeSolv		Lipophilicity		Recon.
	SVM	MLP	SVM	MLP	SVM	MLP	
MIM (1 × 512)	0.65	0.34	2.23	1.82	0.663	0.61	100%
cMIM (1 × 512)	0.47	0.19	2.32	1.67	0.546	0.38	100%
MIM (1 × 512) info emb	0.21	0.29	1.55	1.4	0.234	0.28	100%
cMIM (1 × 512) info emb	0.21	0.24	1.74	1.35	0.24	0.23	100%
CDDD (512)	<b>0.33</b>		<b>0.94</b>		<b>0.4</b>		
†Seq2seq (N × 512)	0.37	0.43	1.24	1.4	0.46	0.61	100%
†Perceiver (4 × 512)	0.4	0.36	1.22	1.05	0.48	0.47	100%
†VAE (4 × 512)	0.55	0.49	1.65	3.3	0.63	0.55	46%
MIM (1 × 512)	0.58	0.54	1.95	1.9	0.66	0.62	100%
Morgan fingerprints (512)	1.52	1.26	5.09	3.94	0.63	0.61	

Table 2: Comparison of models on ESOL, FreeSolv, and Lipophilicity using SVM and MLP regressors, with reconstruction accuracy. Top: our results. Bottom: results from Reidenbach et al. [2023]. For †models, sequence representations were averaged to 512 dimensions. Bold: best non-MIM results. Highlighted: best among MIM-based models. Note that CDDD training included these classification tasks.

**Image Classification.** We trained MIM, cMIM, VAE, cVAE (VAE + cMIM contrastive loss term), and InfoNCE across batch sizes {2, 5, 10, 100, 200}. All models share the same architecture, with InfoNCE consisting only of the encoder. Checkpoints with the lowest validation loss were evaluated on test sets. This design controls for architecture, optimizer, training steps, and dataset usage, isolating the effect of the objective.

We report results using KNN (cosine and Euclidean) and a one-hidden-layer MLP with 400 dimensions. We use Scikit-learn Pedregosa et al. [2011] with default values. Inputs to classifiers are either the mean encoding (standard embedding) or informative embeddings (Section 2.3). Together we

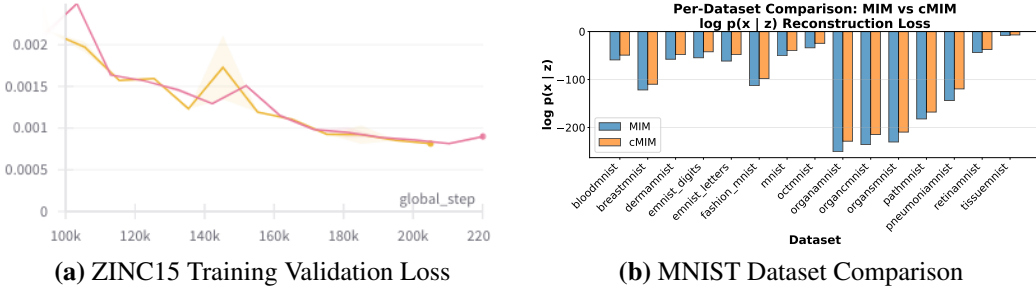


Figure 7: Reconstruction performance of MIM and cMIM. **(a)** Validation reconstruction loss during training on molecular data (cMIM in yellow, MIM in pink) shows comparable behavior. **(b)** Per-dataset test reconstruction log-likelihood on MNIST-like datasets. Surprisingly, cMIM achieves better average reconstruction (-96.25) compared to MIM (-109.64), a +12.2% relative improvement, suggesting a beneficial regularization effect.

evaluate 6 classification tasks per model and batch size. Performance is summarized with (1) average normalized accuracy (z-score across datasets and tasks) and (2) average ranking per dataset and task (Fig. 5).

cMIM consistently outperformed all baselines across batch sizes and metrics, dominating the ranking plots. Both MIM and cMIM surpassed VAE, cVAE, and most InfoNCE runs in z-score. The only competitive non-MIM model was InfoNCE with batch size 100. Adding a contrastive term to VAE (cVAE) had little impact, indicating that cMIM’s advantage arises from combining MIM’s clustering with angular separation.

**Molecular Property Prediction and Informative Embeddings.** Table 2 compares MIM and cMIM on ESOL, FreeSolv, and Lipophilicity tasks. We evaluate SVM and MLP regressors trained on embeddings and informative embeddings. Baselines include CDDD Winter et al. [2019], Seq2seq, Perceiver, VAE, and Morgan fingerprints. We note that CDDD was trained with the classification tasks during training.

cMIM with informative embeddings outperformed vanilla MIM and was competitive with or superior to these baselines. This highlights the value of informative embeddings and the discriminative structure encouraged by cMIM.

### 3.4 Batch Size Sensitivity

Fig. 6 summarizes batch size sensitivity for MIM, cMIM, VAE, cVAE, and InfoNCE. For each model, we performed a linear regression of average z-score on batch size, across six evaluation settings (three classifiers  $\times$  two embedding types). The slope of this fit serves as a measure of sensitivity: positive slope means higher accuracy with larger batches, while near-zero slope indicates robustness.

InfoNCE shows clear dependence on batch size, with positive slopes and low variance. MIM and cMIM both yield slopes near zero with small variance, confirming their robustness to batch size. By contrast, VAE and cVAE exhibit high variance in slopes, reflecting unstable performance and strong sensitivity to batch size changes.

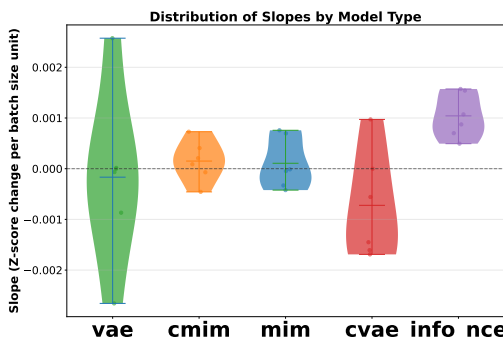


Figure 6: Distribution of slopes from linear fits of accuracy vs. batch size for different models. Each point corresponds to average z-score of a model trained on MNIST-like datasets.

### 3.5 Reconstruction

Fig. 7 compares reconstruction quality of MIM and cMIM. On molecular data (panel **a**), both models exhibit nearly identical reconstruction loss trajectories during training. On MNIST-like datasets (panel **b**), test log-likelihood reveals a consistent advantage for cMIM, which outperforms MIM by an average margin of 12.2%. This improvement was unexpected, as both methods share the same generative architecture. We conjecture that the gain to the implicit regularization can be attributed to the contrastive term, which could reduce overfitting while maintaining generative fidelity.

## 4 Related Work

**Contrastive Learning.** Contrastive learning has become a cornerstone of self-supervised representation learning, with methods such as CPC van den Oord et al. [2018], SimCLR Chen et al. [2020], and MoCo He et al. [2020] demonstrating strong discriminative performance. These approaches typically rely on data augmentation to form positive pairs, making their success dependent on carefully chosen invariances. Augmentation-free contrastive methods, such as BYOL Grill et al. [2020] and SimSiam Chen and He [2021], avoid negatives but often require additional predictors or asymmetries for stability. Our work differs by integrating contrastive learning directly into a probabilistic framework, eliminating the need for augmentation or auxiliary networks.

**Mutual Information Maximization.** The Mutual Information Machine (MIM) Livne et al. [2019] and follow-up works Reidenbach et al. [2023] maximize mutual information between inputs and latent codes while encouraging latent clustering. Related approaches such as Deep InfoMax Hjelm et al. [2018] and InfoVAE Zhao et al. [2017] also maximize information-theoretic quantities, but typically lack a generative auto-encoding structure, or require various approximations and weighted losses which are hard to tune. Our method extends MIM with a contrastive component, addressing its limited discriminative power.

**Informative Embeddings.** Extracting hidden states from encoder–decoder models has proven effective in large language models Brown et al. [2020], Lee et al. [2024]. Similarly, representations from intermediate layers of auto-encoders or VAEs have been used for downstream prediction tasks Alemi et al. [2018]. We generalize this idea by introducing *informative embeddings*, a systematic method to leverage decoder hidden states in probabilistic auto-encoders, demonstrating significant gains in both image and molecular tasks.

**Unifying Generative and Discriminative Learning.** Bridging generative modeling with discriminative performance has been a longstanding goal, explored in frameworks such as  $\beta$ -VAE Higgins et al. [2017], InfoGAN Chen et al. [2016], and hybrid likelihood–contrastive models van den Oord et al. [2018]. Our work contributes to this line by showing that cMIM yields a single framework that maintains generative fidelity while significantly improving discriminative utility.

## 5 Limitations

While cMIM demonstrates clear benefits in discriminative performance and robustness to batch size, several limitations remain. First, we evaluate generative capacity primarily through reconstruction, leaving open the question of how cMIM performs on challenging generative tasks such as sample quality, diversity, likelihood estimation, or controlled generation. Second, our empirical validation is restricted to moderate-scale models and datasets; it remains to be seen how the method scales to larger architectures and high-dimensional modalities such as video or long-context language. Third, although cMIM removes the need for data augmentation, the choice of similarity function and temperature parameter  $\tau$  may still influence results and require tuning. Finally, while we highlight reduced sensitivity to batch size, the method continues to benefit from larger effective numbers of negatives, which can introduce computational overhead when using memory queues or very large batches. These limitations motivate future work in scaling cMIM, expanding to more modalities, and further analyzing its generative behavior.

## 6 Conclusions

In this paper, we introduced cMIM, a contrastive extension of the MIM framework. Unlike conventional contrastive learning, cMIM does not require positive data augmentation and exhibits reduced sensitivity to batch size compared to InfoNCE. Our experiments show that cMIM learns more discriminative features than both MIM and InfoNCE, and consistently outperforms MIM in classification and regression tasks. Moreover, cMIM maintains comparable reconstruction quality to MIM, suggesting similar performance for generative applications, though further empirical validation is needed.

We also proposed a method for extracting embeddings from encoder–decoder models, termed *informative embeddings*, which improve the effectiveness of the learned representations in downstream applications.

Overall, cMIM advances the goal of unifying discriminative and generative representation learning. We hope this work provides a foundation for developing models that excel across a broad spectrum of machine learning tasks and motivates further research in this direction.

## References

Alexander Alemi, Ben Poole, Ian Fischer, Joshua Dillon, Rif A. Saurous, and Kevin Murphy. Fixing a broken elbo. In *International Conference on Machine Learning (ICML)*, pages 159–168, 2018.

Yoshua Bengio, Li Yao, Guillaume Alain, and Pascal Vincent. Generalized denoising auto-encoders as generative models. *arXiv preprint arXiv:1305.6663*, 2013.

Steven Bird, Ewan Klein, and Edward Loper. *Natural Language Processing with Python: Analyzing Text with the Natural Language Toolkit*. O'Reilly Media, Inc., 2009.

Tom B. Brown, Benjamin Mann, Nick Ryder, Melanie Subbiah, Jared Kaplan, Prafulla Dhariwal, Arvind Neelakantan, Pranav Shyam, Girish Sastry, Amanda Askell, et al. Language models are few-shot learners. *arXiv preprint arXiv:2005.14165*, 2020.

Ting Chen, Simon Kornblith, Mohammad Norouzi, and Geoffrey E. Hinton. A simple framework for contrastive learning of visual representations. *arXiv preprint arXiv:2002.05709*, 2020.

Xi Chen, Yan Duan, Rein Houthooft, John Schulman, Ilya Sutskever, and Pieter Abbeel. Infogan: Interpretable representation learning by information maximizing generative adversarial nets. In *Advances in Neural Information Processing Systems (NeurIPS)*, pages 2172–2180, 2016.

Xinlei Chen and Kaiming He. Exploring simple siamese representation learning. *arXiv preprint arXiv:2011.10566*, 2021.

Gregory Cohen, Saeed Afshar, Jonathan Tapson, and André van Schaik. EMNIST: an extension of MNIST to handwritten letters. *CoRR*, abs/1702.05373, 2017. URL <http://arxiv.org/abs/1702.05373>.

Li Deng. The mnist database of handwritten digit images for machine learning research [best of the web]. *IEEE Signal Processing Magazine*, 29(6):141–142, 2012. doi: 10.1109/MSP.2012.2211477.

Jacob Devlin, Ming-Wei Chang, Kenton Lee, and Kristina Toutanova. Bert: Pre-training of deep bidirectional transformers for language understanding. *arXiv preprint arXiv:1810.04805*, 2018.

Jean-Bastien Grill, Florian Strub, Florent Altché, Corentin Tallec, Pierre H. Richemond, Elena Buchatskaya, Carl Doersch, Bernardo Ávila Pires, Zhaohan Daniel Guo, Mohammad Gheshlaghi Azar, Bilal Piot, Koray Kavukcuoglu, Rémi Munos, and Michal Valko. Bootstrap your own latent: A new approach to self-supervised learning. *arXiv preprint arXiv:2006.07733*, 2020.

Kaiming He, Haoqi Fan, Yuxin Wu, Saining Xie, and Ross Girshick. Momentum contrast for unsupervised visual representation learning. In *Proceedings of the IEEE/CVF Conference on Computer Vision and Pattern Recognition (CVPR)*, pages 9729–9738, 2020.

Irina Higgins, Loic Matthey, Arka Pal, Christopher Burgess, Xavier Glorot, Matthew Botvinick, Shakir Mohamed, and Alexander Lerchner.  $\beta$ -VAE: Learning Basic Visual Concepts with a Constrained Variational Framework. In *International Conference on Learning Representations (ICLR)*, 2017.

R. Devon Hjelm, Alex Fedorov, Samuel Lavoie-Marchildon, Khurram Grewal, Philip Bachman, Adam Trischler, and Yoshua Bengio. Learning deep representations by mutual information estimation and maximization. *arXiv preprint arXiv:1808.06670*, 2018.

Wassily Hoeffding. Probability inequalities for sums of bounded random variables. *Journal of the American Statistical Association*, 58(301):13–30, March 1963. URL <http://www.jstor.org/stable/2282952>.

Shengding Hu, Yuge Tu, Xu Han, Chaoqun He, Ganqu Cui, Xiang Long, Zhi Zheng, Yewei Fang, Yuxiang Huang, Weilin Zhao, et al. Minicpm: Unveiling the potential of small language models with scalable training strategies. *arXiv preprint arXiv:2404.06395*, 2024.

Ross Irwin, Spyridon Dimitriadis, Jiazen He, and Esben Jannik Bjerrum. Chemformer: a pre-trained transformer for computational chemistry. *Machine Learning: Science and Technology*, 3(1):015022, 2022. doi: 10.1088/2632-2153/ac3ffb. URL <https://doi.org/10.1088/2632-2153/ac3ffb>.

Andrew Jaegle, Felix Gimeno, Andy Brock, Oriol Vinyals, Andrew Zisserman, and Joao Carreira. Perceiver: General perception with iterative attention. In *International Conference on Machine Learning (ICML)*, volume 139 of *Proceedings of Machine Learning Research*, pages 4651–4664. PMLR, 2021.

Sunghwan Kim, Jie Chen, Tiejun Cheng, Asta Gindulyte, Jia He, Siqian He, Qingliang Li, Benjamin A. Shoemaker, Paul A. Thiessen, Bo Yu, Leonid Zaslavsky, Jian Zhang, and Evan E. Bolton. Pubchem 2019 update: improved access to chemical data. *Nucleic Acids Research*, 47(D1):D1102–D1109, 2018. doi: 10.1093/nar/gky1033. URL <https://doi.org/10.1093/nar/gky1033>.

Diederik P. Kingma and Jimmy Ba. Adam: A method for stochastic optimization. In *International Conference on Learning Representations (ICLR)*, 2015.

Oleksii Kuchaiev, Jason Li, Huyen Nguyen, Oleksii Hrinchuk, Ryan Leary, Boris Ginsburg, Samuel Kriman, Stanislav Beliaev, Vitaly Lavrukhin, Jack Cook, et al. Nemo: a toolkit for building ai applications using neural modules. *arXiv preprint arXiv:1909.09577*, 2019.

Phuc H. Le-Khac, Graham Healy, and Alan F. Smeaton. Contrastive representation learning: A framework and review. *arXiv preprint arXiv:2010.05113*, 2020.

Chankyu Lee, Rajarshi Roy, Mengyao Xu, Jonathan Raiman, Mohammad Shoeybi, Bryan Catanzaro, and Wei Ping. Nv-embed: Improved techniques for training llms as generalist embedding models. *arXiv preprint arXiv:2405.17428*, 2024.

Micha Livne, Kevin Swersky, and David J. Fleet. MIM: Mutual Information Machine. *arXiv preprint arXiv:1910.03175*, 2019.

Micha Livne, Kevin Swersky, and David J Fleet. Sentencemim: A latent variable language model. *arXiv preprint arXiv:2003.02645*, 2020.

Fabian Pedregosa, Gaël Varoquaux, Alexandre Gramfort, Vincent Michel, Bertrand Thirion, Olivier Grisel, Mathieu Blondel, Peter Prettenhofer, Ron Weiss, Vincent Dubourg, Jake Vanderplas, Alexandre Passos, David Cournapeau, Matthieu Brucher, Matthieu Perrot, and Édouard Duchesnay. Scikit-learn: Machine learning in python. *Journal of Machine Learning Research*, 12(85):2825–2830, 2011. URL <http://jmlr.org/papers/v12/pedregosa11a.html>.

Danny Reidenbach, Micha Livne, Rajesh K. Ilango, Michelle Gill, and Johnny Israeli. Improving small molecule generation using mutual information machine. *arXiv preprint arXiv:2208.09016*, 2023.

Teague Sterling and John J. Irwin. Zinc 15 – ligand discovery for everyone. *Journal of Chemical Information and Modeling*, 55(11):2324–2337, 2015. doi: 10.1021/acs.jcim.5b00559. URL <https://doi.org/10.1021/acs.jcim.5b00559>.

Aäron van den Oord, Yazhe Li, and Oriol Vinyals. Representation learning with contrastive predictive coding. *arXiv preprint arXiv:1807.03748*, 2018.

Ashish Vaswani, Noam Shazeer, Niki Parmar, Jakob Uszkoreit, Llion Jones, Aidan N. Gomez, Łukasz Kaiser, and Illia Polosukhin. Attention is all you need. In *Advances in Neural Information Processing Systems (NeurIPS)*, volume 30, 2017.

Tongzhou Wang and Phillip Isola. Understanding contrastive representation learning through alignment and uniformity on the hypersphere. In *Proceedings of the 37th International Conference on Machine Learning (ICML)*, pages 9929–9939. PMLR, 2020.

David Weininger. Smiles, a chemical language and information system. 1. introduction to methodology and encoding rules. *Journal of Chemical Information and Computer Sciences*, 28(1):31–36, 1988. doi: 10.1021/ci00057a005. URL <https://doi.org/10.1021/ci00057a005>.

Robin Winter, Floriane Montanari, Frank Noé, and Djork-Arné Clevert. Learning continuous and data-driven molecular descriptors by translating equivalent chemical representations. *Chemical Science*, 10:1692–1701, 2019. doi: 10.1039/C8SC04175J. URL <http://dx.doi.org/10.1039/C8SC04175J>.

Jiancheng Yang, Rui Shi, Donglai Wei, Zequan Liu, Lin Zhao, Bilian Ke, Hanspeter Pfister, and Bingbing Ni. Medmnist v2: A large-scale lightweight benchmark for 2d and 3d biomedical image classification. *CoRR*, abs/2110.14795, 2021. URL <https://arxiv.org/abs/2110.14795>.

Xianlong Zeng, Fanghao Song, and Ang Liu. Similar data points identification with llm: A human-in-the-loop strategy using summarization and hidden state insights. *arXiv preprint arXiv:2404.04281*, 2024.

Shengjia Zhao, Jiaming Song, and Stefano Ermon. Infovae: Information maximizing variational autoencoders. In *Proceedings of the Thirty-First AAAI Conference on Artificial Intelligence*, pages 5885–5892, 2017.

## A Experiment Training Details

### A.1 Image Classification

We opted for a simple architecture.

- The encoder flattens the image to 784 dimensions, up-projects using a linear layer to (784, 16) which is fed to a Perceiver encoder that projects it down to 400 steps (400, 16). A linear layer projects the hidden dimension to 1, followed by a layer norm, and finally a linear projection from 400 to 64.
- The encoding distribution is a Gaussian with mean and variance predicted by linear layers from the encoder output.
- The decoder up-projects the 64 dimension latent code using a linear layer to (64, 16) which is fed to a Perceiver encoder that projects it down to 400 steps (400, 16). A linear layer projects the hidden dimension to 1, followed by a layer norm, and finally a linear projection from 400 to 784, which is reshaped back to (28, 28) image dimensions.
- The decoding distribution is a conditional Bernoulli with logits predicted by a linear layer from the decoder output.
- The prior is a standard Gaussian.

All models were trained with Adam optimizer with learning rate  $1e - 3$  and WSD scheduler with 10% warmup steps and 10% decay steps, for a total of 500k steps (regardless of the batch size).

### A.2 Moleculal Property Prediction

**Dataset:** All models were trained using a tranche of the ZINC-15 dataset [Sterling and Irwin, 2015], labeled as reactive and annotated, with molecular weight  $\leq 500\text{Da}$  and  $\text{logP} \leq 5$ . Of these molecules, 730M were selected at random and split into training, testing, and validation sets, with 723M molecules in the training set. We note that we do not explore the effect of model size, hyperparameters, and data on the models. Instead, we train all models on the same data using the

same hyperparameters, focusing on the effect of the learning framework and the fixed-size bottleneck. For comparison, Chemformer was trained on 100M molecules from ZINC-15 [Sterling and Irwin, 2015] – 20X the size of the dataset used to train CDDD (72M from ZINC-15 and PubChem [Kim et al., 2018]). MoLFormer-XL was trained on 1.1 billion molecules from the PubChem and ZINC datasets.

**Data augmentation:** Following Irwin et al. [2022], we used two augmentation methods: masking, and SMILES enumeration [Weininger, 1988]. Masking is as described for the BART MLM denoising objective, with 10% of the tokens being masked, and was only used during the training of MegaMolBART. In addition, MegaMolBART, PerBART, and MolVAE used SMILES enumeration where the encoder and decoder received different valid permutations of the input SMILES string. MolMIM was the only model to see an increase in performance when both the encoder and decoder received the same input SMILES permutation, simplifying the training procedure.

**Model details:** We implemented all models with NeMo Megatron toolkit [Kuchaiev et al., 2019]. We used a RegEx tokenizer with 523 tokens [Bird et al., 2009]. All models had 6 layers in the encoder and 6 layers in the decoder, with a hidden size of 512, 8 attention heads, and a feed-forward dimension of 2048. The Perceiver-based models also required defining  $K$ , the hidden length, which relates to the hidden dimension by  $H = K \times D$  where  $H$  is the total hidden dimension, and  $D$  is the model dimension (Fig. 3). MegaMolBART had  $58.9M$  parameters, PerBART had  $64.6M$ , and MolVAE and MolMIM had  $65.2M$ . We used greedy decoding in all experiments. We note that we trained MolVAE using the loss of  $\beta$ -VAE [Higgins et al., 2017] where we scaled the KL divergence term with  $\beta = \frac{1}{D}$  where  $D$  is the hidden dimensions.

**Optimization:** We use ADAM optimizer [Kingma and Ba, 2015] with a learning rate of 1.0, betas of 0.9 and 0.999, weight decay of 0.0, and an epsilon value of 1.0e-8. We used Noam learning rate scheduler [Vaswani et al., 2017] with a warm-up ratio of 0.008, and a minimum learning rate of 1e-5. During training, we used a maximum sequence length of 512, dropout of 0.1, local batch size of 256, and global batch size of 16384. All models were trained for 1,000,000 steps with fp16 precision for 40 hours on 4 nodes with 16 GPU/node (Tesla V100 32GB). MolVAE was trained using  $\beta$ -VAE [Higgins et al., 2017] with  $\beta = \frac{1}{H}$  where  $H$  is the number of hidden dimensions. We have found this choice to provide a reasonable balance between the rate and distortion (see Alemi et al. [2018] for details). It is important to note that MolMIM does not require the same  $\beta$  hyperparameter tuning as done for VAE.

## B Additional Results

### B.1 MNIST-like Image Classification

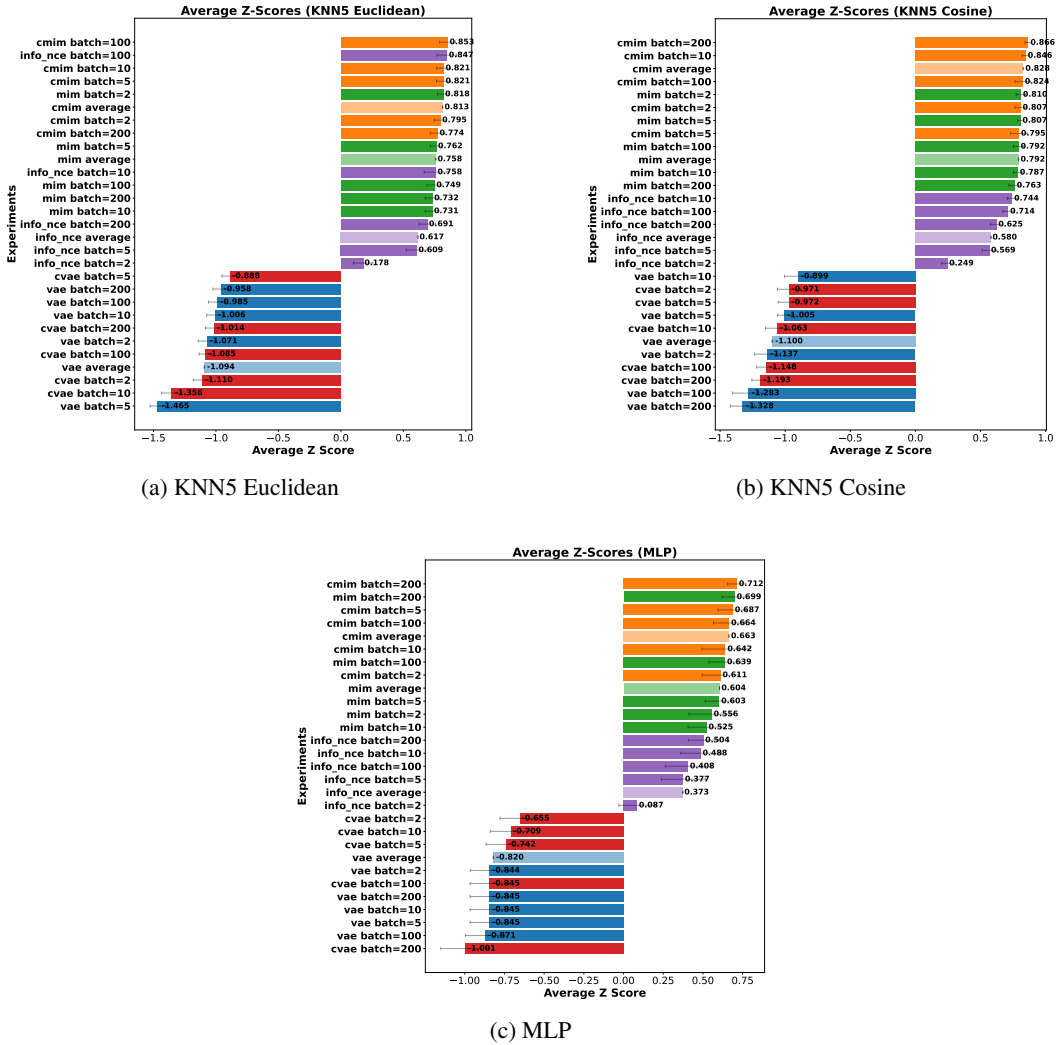


Figure 8: Z-scores with error bars for MNIST-like image classification tasks using different evaluation methods.

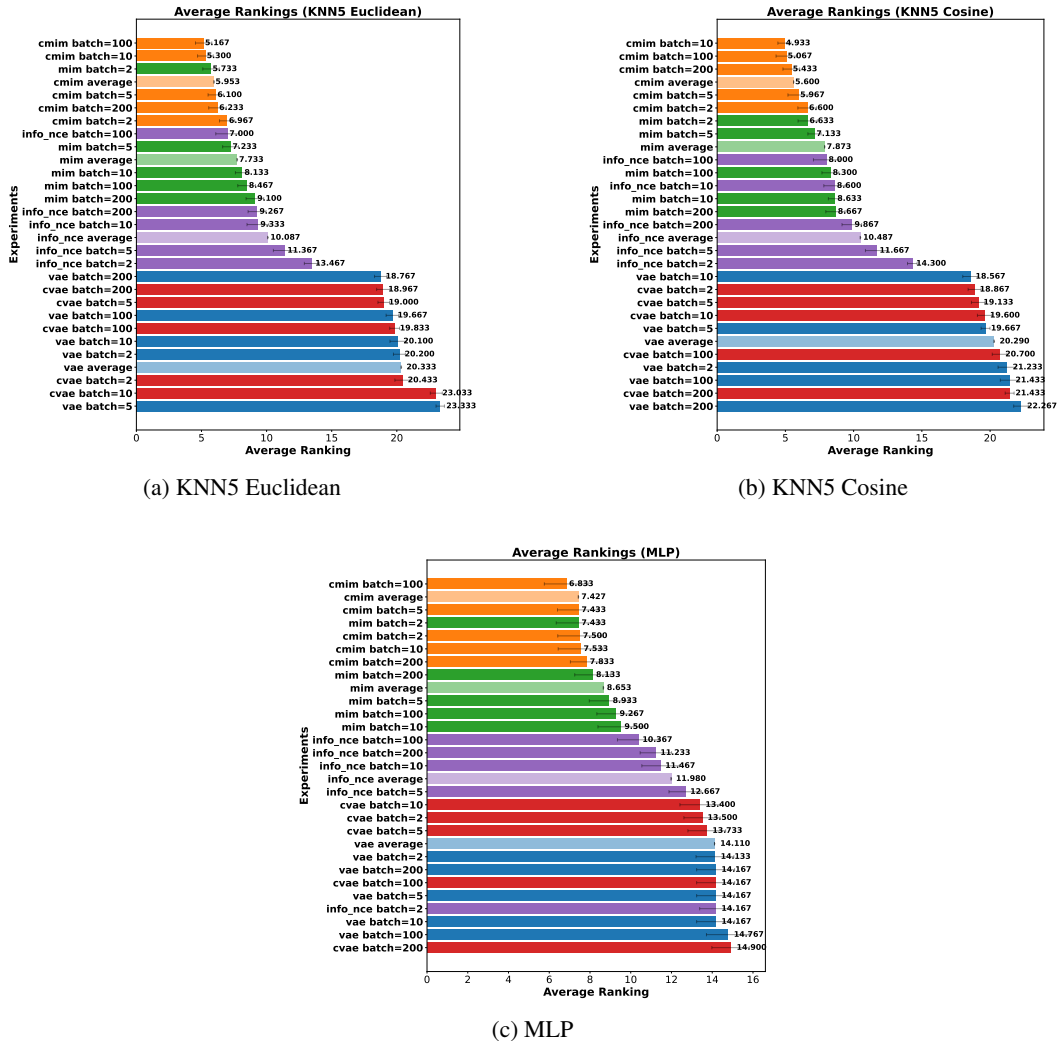


Figure 9: Rankings with error bars for MNIST-like image classification tasks using different evaluation methods.